# Drone Magnetometry in Mining Research. An Application in the Study of Triassic Cu–Co–Ni Mineralizations in the Estancias Mountain Range, Almería (Spain)

Daniel Porras [1], Javier Carrasco [2], Pedro Carrasco [3], Santiago Alfageme [4], Diego Gonzalez-Aguilera [3,*] and Rafael Lopez Guijarro [5]

1   Geoland Services S.L., 28008 Madrid, Spain; dporras@geoland.es
2   Técnicas Geofísicas S.L., 05003 Avila, Spain; tgeofisicas@gmail.com
3   Departamento Ingeniería Cartográfica y del Terreno Geología, Escuela Politécnica Superior de Ávila, Universidad de Salamanca, Avd. Hornos Caleros 50, 05003 Avila, Spain; retep81@usal.es
4   Gesminle S.L., 24001 Leon, Spain; sca@gesminle.es
5   Exco Mining S.L., 28008 Madrid, Spain; rlopez@excomining.es
*   Correspondence: daguilera@usal.es; Tel.: +34-920353500

**Abstract:** The use of drones in mining and geological exploration is under rapid development, especially in the field of magnetic field prospection. In part, this is related to the advantages presented for over ground surveys, allowing for high-density data acquisition with low loss of resolution, while being particularly useful in scenarios where vegetation, topography, and access are limiting factors. This work analyzes results of a drone magnetic survey acquired across the old mines of Don Jacobo, where Copper-Cobalt-Nickel stratabound mineralizations were exploited in the Estancias mountain range of the Betic Cordillera, Spain. The survey carried out used a vapor magnetometer installed on a Matrice 600 Pro Hexacopter. Twenty-four parallel survey lines were flown with a speed of 5 m/s, orthogonal to the regional strike of the geological structure, and mineralization with 50 m line separation and 20 m flight height over the ground was studied. The interpretation of the magnetic data allows us to reveal and model two high magnetic susceptibility bodies with residual magnetization, close to the old mines and surface mineral shows. These bodies could be related to potential unexploited mineralized areas whose formation may be related to a normal fault placed to the south of the survey area. Our geophysical survey provides essential data to improve the geological and mining potential of the area, allowing to design future research activities.

**Keywords:** aeromagnetics; drone survey; mineral exploration; geophysical prospecting

## 1. Introduction

The demand for raw materials is rapidly increasing, proving a fundamental pillar in modern development as well as the future prospects of European industries. The product of this is a rise in demand for new material extraction sites that are able to support this type of development. In the case of Europe, geological and mining research is currently hindered by the effectiveness and speed of traditional methodologies in this type of research. This has resulted in adaptations in the field of geophysics in response to increasingly stricter requirements.

In this context, the use of drones is under important development, incorporating more autonomous systems allowing for the integration of multiple sensors such as: RGB sensors, ultrasonic sensors, Infrared Sensors (IR), stereo camera, laser range finders (LRFs), Ultra-Wideband Radar (UWB), and hyperspectral sensors like hyperspectral cameras, which allows for its use in a variety of civilian and military applications [1,2] and missions including the magnetometer for geological and mining research [3–9]. Other authors have used drone magnetometry in the oil and gas industry to locate abandoned wells and other

buried infrastructures such as pipelines over wide areas [10–12]. Traditionally, magnetic surveys are performed on-site moving the sensor manually, thus capturing high resolution spatial data at the cost of low productivity. These approaches are additionally limited by access to the area of study. Other approaches consist in the installation of sensors on planes, increasing productivity by being able to study larger areas in smaller periods of time, at the cost of spatial resolution [13]. The use of drones is thus an alternative of interest presenting multiple operative advantages, such as flexibility, ease of use, and a lower logistic cost. Additionally, drones present high capacity for obtaining data over large areas in short periods of time, with less restrictions based on low accessibility, topographical, environmental, and vegetative conditions.

One of the most common techniques used in geological and mining research is magnetometry, employing the use of specially designed sensors that can be made airborne using drones [14–16]. This consists of a means of remotely carrying out geophysical surveys based on the measurement of terrestrial magnetic variations at regular intervals along a set of profiles. The majority of minerals present their own particular non-magnetic behavior. Nevertheless, another group of minerals exists, called ferromagnectic minerals, which include the cobalt ores frequently found in the Estancias mountain range of the Betic Cordillera, Spain, whose concentration in the Earth's crust generates detectable local variations in the magnetic field.

The present research project is focused on the analysis of the Don Jacobo mine, where copper and cobalt minerals were found in Triassic carbonates and have been extracted since the mid-19th century, up to the beginning of the 21st century [17]. These minerals include azurite, malachite, limonite, pyrite, galena, and erythrite. Mining works in the area were limited to small galleries that penetrated only few meters into the rock. There are no data from previous geophysical surveys or drilling activities.

This study thus has the primary objective of extracting information from this area in relation to the possible presence of mineral bodies located under areas of complex topographies where high slopes, scree debris, and vegetation make the application of ground geophysical techniques difficult. It is known that these topographic particularities make it difficult to study this area using other ground geophysical techniques such as, for example, electrical tomography, induced polarization, and ground magnetometry, which highlights the importance of research with drones in this application.

## 2. Geological Context and General Characteristics of the Locality

The region of interest is located in the Estancias mountain range, in the southeastern part of the Iberian peninsula, geologically positioned in the northern region of the Internal Betic Cordillera (Figure 1A), in materials of the The Alpujárride Complex, belonging to the Internal Zones of the Betic Cordillera. The diverse lithologies present can be organized into three large lithological units defining this complex. Stratigraphically, these three units correspond with, from bottom to top: Paleozoic shales, Triassic phyllite-quartzites, and Triassic carbonates (dolomitic-limestone). The first two units are additionally affected by Alpine metamorphism.

These units are presented with a general east-west orientation (N75-90E) (Figure 1B), conditioned by a strong deformation due to tectonic accidents [18,19]. These accidents have been interpreted mostly as fault propagation folds towards the south/south-east [20], thus conditioning the geological structures within this region (Figure 1B,C).

The area occupied by the Don Jacobo mine, and the general location of the target minerals, are dispersed in a topographically abrupt region, positioned on a 1000 m by 300 m (length × width) portion of the Triassic dolomitic-limestone unit. This unit is located above phyllites and is constricted towards the south by an interpreted as a possible normal tertiary fault, partially covered by plio-quaternary materials (Figure 1C).

From a metallogenetic perspective, the mineralizations are located within the Upper Triassic dolomites and limestones of the Alpujarride Complex, and are considered to be stratobound [18]. Rich Co-Cu mineralization can be found here alongside other minor elements

(Ni-Pb-Zn-Ag-Se-As-Hg) [21]. This is similar to the geological-lithological contexts of the Betic region, such as those found in Molvízar (Granada) and Huércal-Overa (Almería).
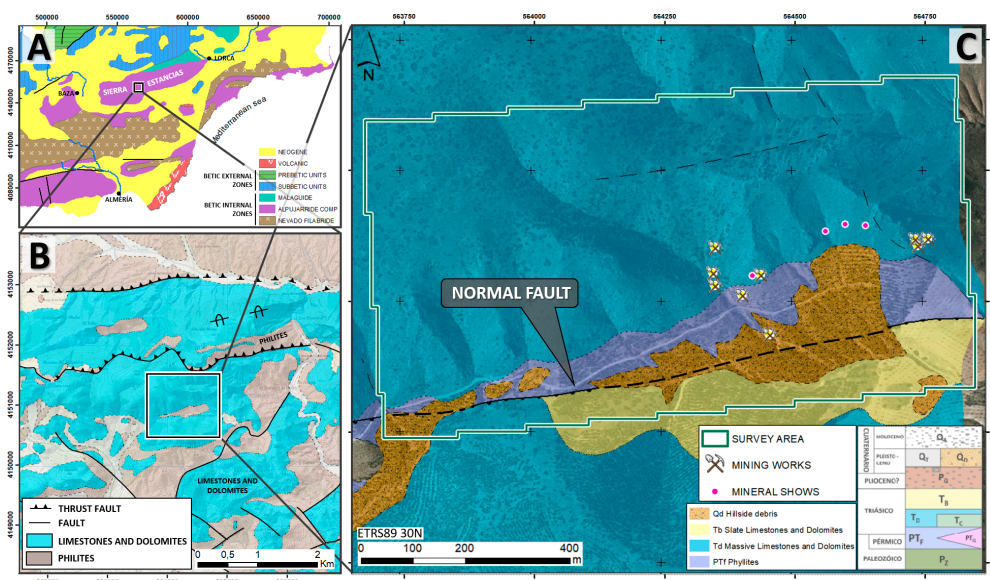


**Figure 1.** (**A**) Geological Context of the southeastern part of the Iberian Peninsula; (**B**) 1:50,000 Geological map (sheet 973—Chirivel and 995—Cantoria, Instituto Geológico y Minero de España, 1972 [18,19]), where the general east-west trend of the Alpujarride Complex can be observed; (**C**) 1:5000 cartographic revision of the Don Jacobo mine area, showing the main tectonic accident in the area (southern normal fault—black dashed line), survey area, and position of the Don Jacobo mines and outcropping mineral shows.

Genetically, these mineralizations have been attributed to a Mississippi Valley type, where metals are a product of the hydrothermal washing of marine series or from mafic intrusions, with carbonates acting as a reducing trap for the mineralization. The carbonated lithologies are constituted by large structures separated among themselves by phyllite lithologies, typically associated with important tectonic accidents. These accidents are then considered the potential channels for hydrothermal circulation [20].

The geochemical studies as well as nearby mineral indices documented from the initial exploitation of the Don Jacobo mine indicate the presence of Cu-Co-Ni primary mineralizations, with the presence of Pb-Zn (Ag), and with Cu and Co contents of >3% and 1%, respectively (Figure 2, [21]). No drilling data or geophysical surveys are available.
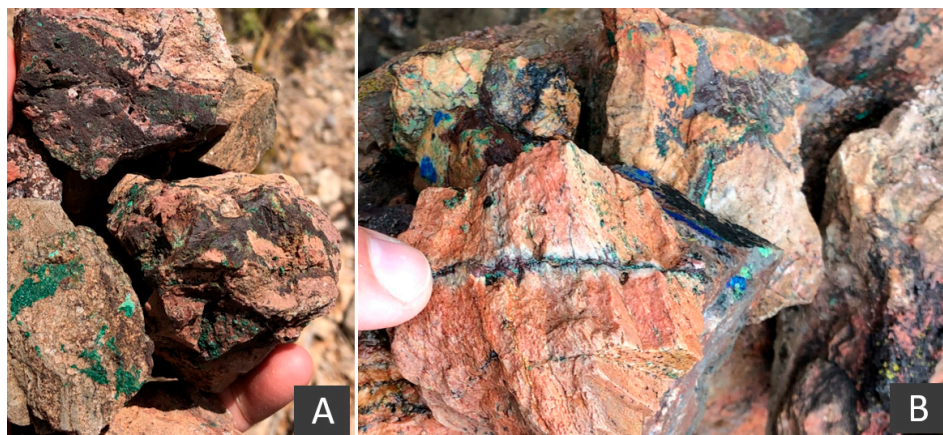


**Figure 2.** Mineralizations of the Don Jacobo mine; (**A**,**B**) Cu carbonates (green and blue colors) and veins of black Co oxides (black colors).

## 3. Materials and Methods

This research project consisted in the analysis of the mine's surroundings and out-cropping mineral shows. Additionally, this research has tried to analyze the carbonated outcrops that appear over the 80 ha area.

### 3.1. Site Conditions

Data collection was performed on 14 June 2020 in warm, sunny, uncloudy, and low wind speed (<16 m/s) day, and lasted a total of 4 h (from 10 am. to 2 pm.). The area under study is practically covered with matorral type shrub-land, and scattered with dense wooded areas (Corine Land Cover 2018 types 312 and 323—https://land.copernicus.eu/pan-european/corine-land-cover/clc2018—accessed on 1 November 2021). The area is accessible by only one track and is characterized by a low anthropogenic magnetic noise area and a severe topography, with an average slope of >26° (Figure 3). To minimize risks such as drone collision with topographic or vegetative elements (the tallest trees in the area reaching approximately 8 m Above Ground Level-AGL) and to ensure flight at a constant height above the ground, a digital elevation model (DEM) of the area was first generated. For this flight, the most important geometric criteria for photogrammetric applications were considered [22], allowing the generation of cartographic data of high quality and obtaining a Ground Sample Distance (GSD) of 4 cm/pixel. This DEM was calculated using a Dji Mavic 2 Pro drone with a 1″ CMOS sensor, flying at 150 m AGL.
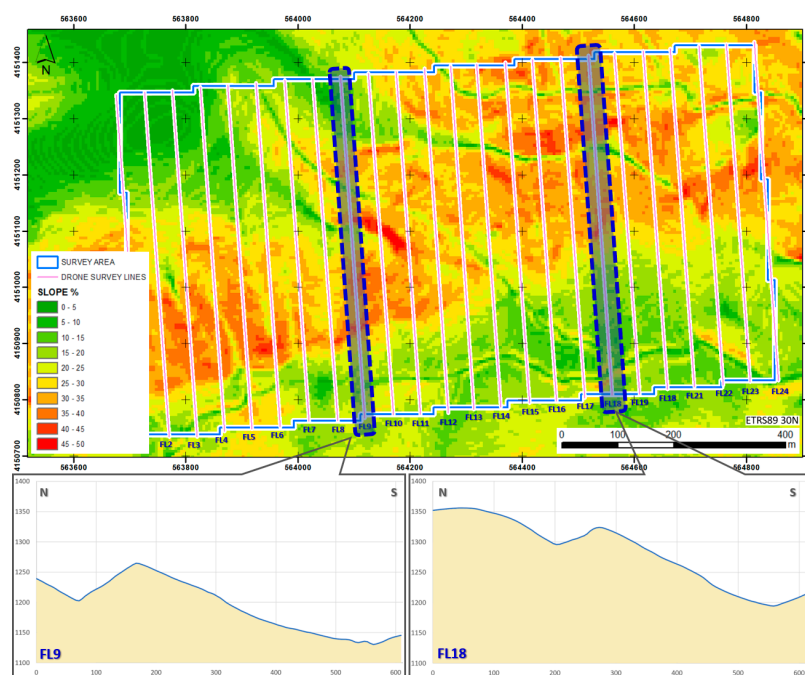


**Figure 3.** Slope map of the study area including drone flight lines (pink lines). The topographic profiles of flight lines 9 (FL9) and 18 (FL18) show the wild topographical characteristics of the area.

### 3.2. Platform and Flight Planning

The platform employed for the present study was the multi-rotor hexacopter Dji Matrice 600 Pro (Figure 5A), equipped with a A3Pro flight controller, and compatible with the UgCS mission planning tool software. This equipment has a total takeoff weight of 9.6 kg, and up to 6 kg payload, while being powered by 6 lithium polymer batteries (4500 mAh).

Flight software (UgCS) was used for the design and control of the survey. Twenty-four 650 m length parallel survey lines were flown trending N170E, orthogonal to the regional strike of the geological structure and mineralization (N75-90E), with a 50 m line separation in order to obtain a high spatial resolution that allows observing variations in the magnetic

field of target size. Due to the extension of the survey area, the total flight was divided into four flight blocks and two take-off and landing points taking into account the capacity of the batteries (Figure 4). The flight was programmed with a speed of 5 m/s and a sampling interval of 200 ms, obtaining measurements every meter along the registered profile. This selected configuration results in a total of 14,500 magnetic total field registration points. The altitude of the flight (20 m AGL) was selected to maximize the resolution of the sensor while guaranteeing safety against obstacles, integrating the DEM acquired previously. A 1 m tolerance level was also used for altitude adjustments.
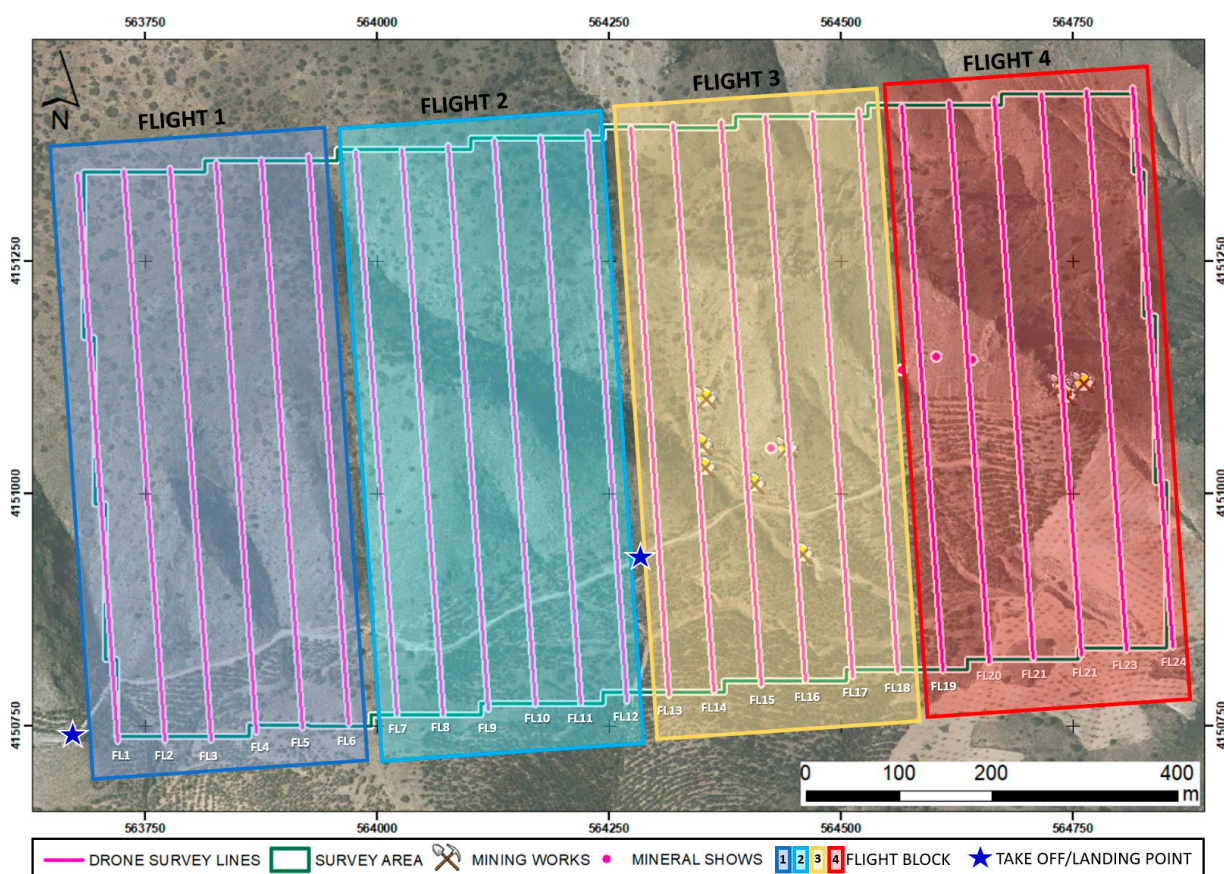


**Figure 4.** Survey design including flight lines (pink lines) and flying blocks division, including the take-off and landing points.

The effect produced by the distance between the sensor and the surface generates a low decrease of spatial resolution and intensity compared to ground surveys [16,23,24], compensated by a regular and higher density data acquisition.

### 3.3. Magnetometry

The drone was equipped with a GSMP-35U GEM-Systems potassium-vapor magnetometer, with a sensibility of 0.0002 nT/1 Hz. This system is additionally equipped with a simultaneous register of the magnetic field, as well as a real-time single-frequency (L1) GPS receiver with up to 0.7 m absolute accuracy in Satellite Based Augmentation System coverage areas.

This equipment consists of a sensor attached by cable to a controller, datalogger, 5 V battery power-source, and GPS, with a total weight of <2 kg. The datalogger and batteries were securely fixed and balanced in the payload container of the drone's undercarriage, while the GPS antenna was installed on the upper portion of the drone, so as to ensure a constant signal. Due to the magnetic interference that is generated by electromagnetic motors within the platform [5,24,25], the magnetic sensor was installed at a 3 m distance from the base of the drone, connected by cable, so as to counteract this electromagnetic

effect (Figure 5B). For this configuration, the magnetic field produced by the drone is attenuated and does not affect the measurements of the GSMP-35U magnetometer [20].
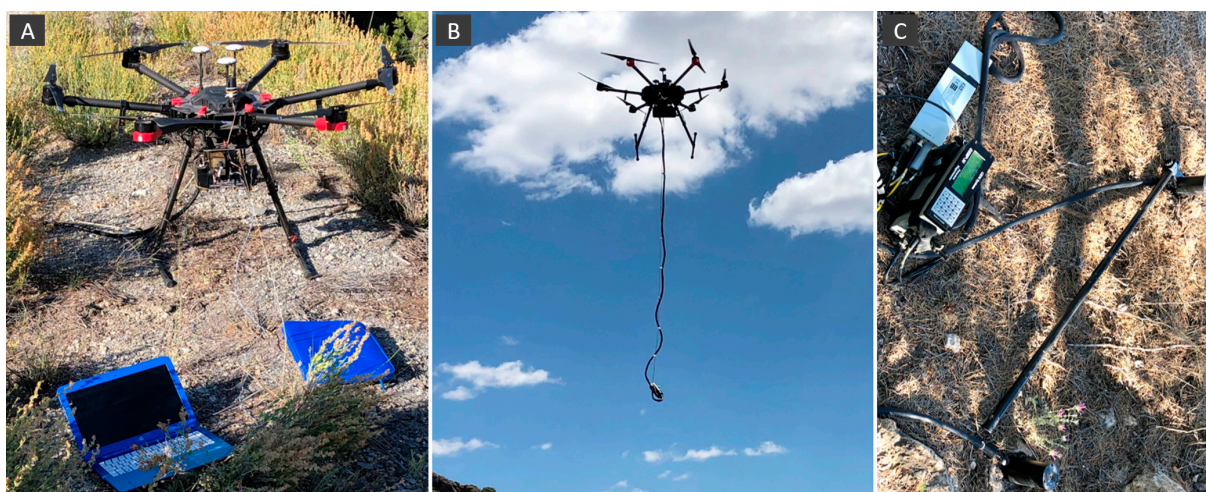


**Figure 5.** Registration system. (**A**) a Mavic Matrice 600 Pro Hexacopter drone; (**B**) static drone position with the magnetometer hanging below; (**C**) base magnetometer for diurnal corrections.

The magnetic sensor was deployed with no rotational restrictions about any of the axes. The survey was designed by adding an extra 25 m at each extremity of the flying lines at the 180° turn and reducing flight speed, preventing the pendulum motion of the sensor that creates yaw, pitch, and roll axis variations.

In parallel, a fixed magnetometer was installed in a nearby area away from sources of magnetic interference to calculate the diurnal effect correction caused by the temporal variation of the magnetic field throughout the day (Figure 5C). The magnetometer was set up with a 1 s time total field interval record, found to register a maximum of 11 nT throughout the data collection period.

### 3.4. Data Processing

Data were processed using the OASIS Montaj 9.8 software, using classic methods in the calculation of anomalies by applying a series of different filters so as to obtain anomaly residual maps. First, erroneous values due to drone position, take-off, landing, pitch, excess roll, and lag errors between the sensor and the drone are deleted. All points placed over the extended extremes of the survey lines and other outliners were discarded, applying a 1D median filter. Finally, diurnal variation of the Earth's magnetic field values caused by sun activity were used to correct the data obtained during the survey period [26].

Aeromagnetic data processing is based on a gridding computation routine that interpolates the observed aeromagnetic data from the survey data, placing these locations into a regular grid with the nodes displayed as a 2D total magnetic field contour map (RGB image). The minimum curvature gridding method was applied to the observed data [27], at $\frac{1}{4}$ of the flight line spacing (12.5 m) [28].

### 4. Results

#### 4.1. Total Magnetic Field (TMF) and Reduction to Pole (TMFRP)

Data interpretation begins with the calculation of the Total Magnetic Field (TMF), from the filtered data (Figure 6A), and the Reduction to Pole (TMFRP). From this perspective, applying the data regarding magnetic inclination and declination of this area on the day of data collection, and in combination with the International Geomagnetic Reference Field (IGRF), a view of the central magnetic sources can be obtained directly for the bodies that generated them (Figure 6B).
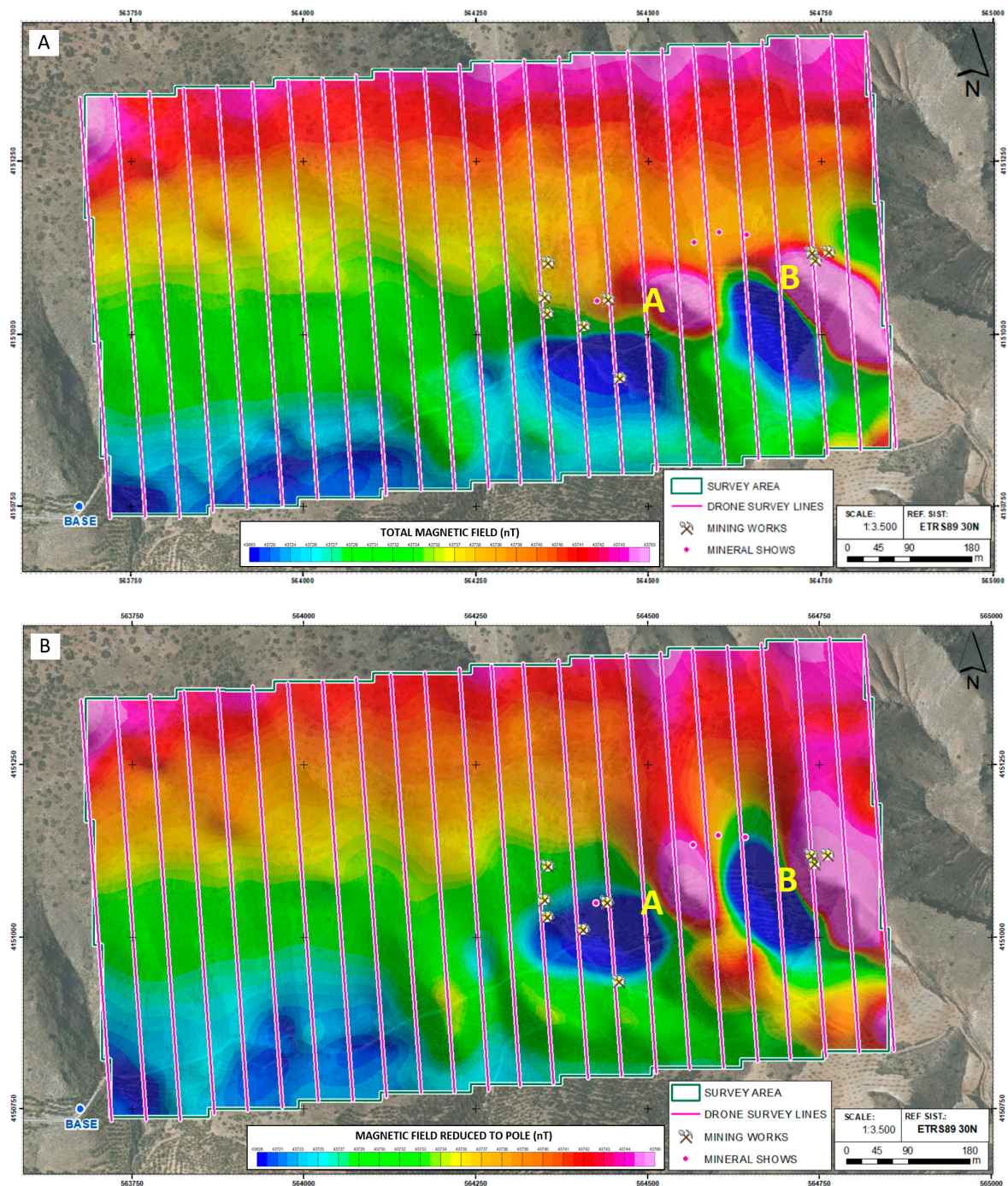
**Figure 6.** (**A**) Total Magnetic Field (TMF) and (**B**) Total Magnetic Field with Reduction to Pole (TMFRP). Dipoles A and B have been marked on each map, as well as the location of different mining activities and areas where the mineralization had been observed on the surface.

On both planes, the presence of two strong magnetic dipoles can be observed (A and B) towards the south-east quadrant of the region of interest. Both dipoles are located on carbonated materials and can be found in the immediate surroundings of the old mine as well as areas where the mineralization had originally been detected on surface.

TMFRP presents a slight variation in the position of the dipoles with reference to the TMF (Figure 6B), as well as an increase in its intensity, reaching a variation in the magnetic field of up to 88 nT (dipole A) and 165 nT (dipole B). The dipoles can be related to the

presence of ferromagnetic elements compatible with the paragenesis of the minerals from this locality.

It is important to point out that reduction to pole has not removed the dipolar character of the magnetic anomalies, which indicates a remaining magnetization of the materials found in this source. This is product of the natural axis of these dipoles, found approximately E-W and not N-S, as would be expected in the actual position of the magnetic field. Under this premise, the mineral bodies that generate these dipoles obtained the remaining magnetization at a moment in time when the magnetic field was different from present day.

### 4.2. Analytical Signal

The filtered Analytical Signal (AS) allows for the spatial identification of the two sources producing the observed dipoles. The calculation of AS is based on the execution of directional derivatives, where the obtained anomalies are organized in a bell-shape, and where the maxima are located directly on the edges of the anomalous bodies, with their amplitude being proportional to the depth of the location of the magnetic source [29].

The map displaying the computed analytical signal (Figure 7) presents a preferential lineation of anomalous areas with an approximate orientation of N80E, coinciding with the two maxima (A and B, Figure 7), and the general trend of the main geological contacts and structures, specially, with the normal fault defined through the geological cartography of the area (Figure 8).
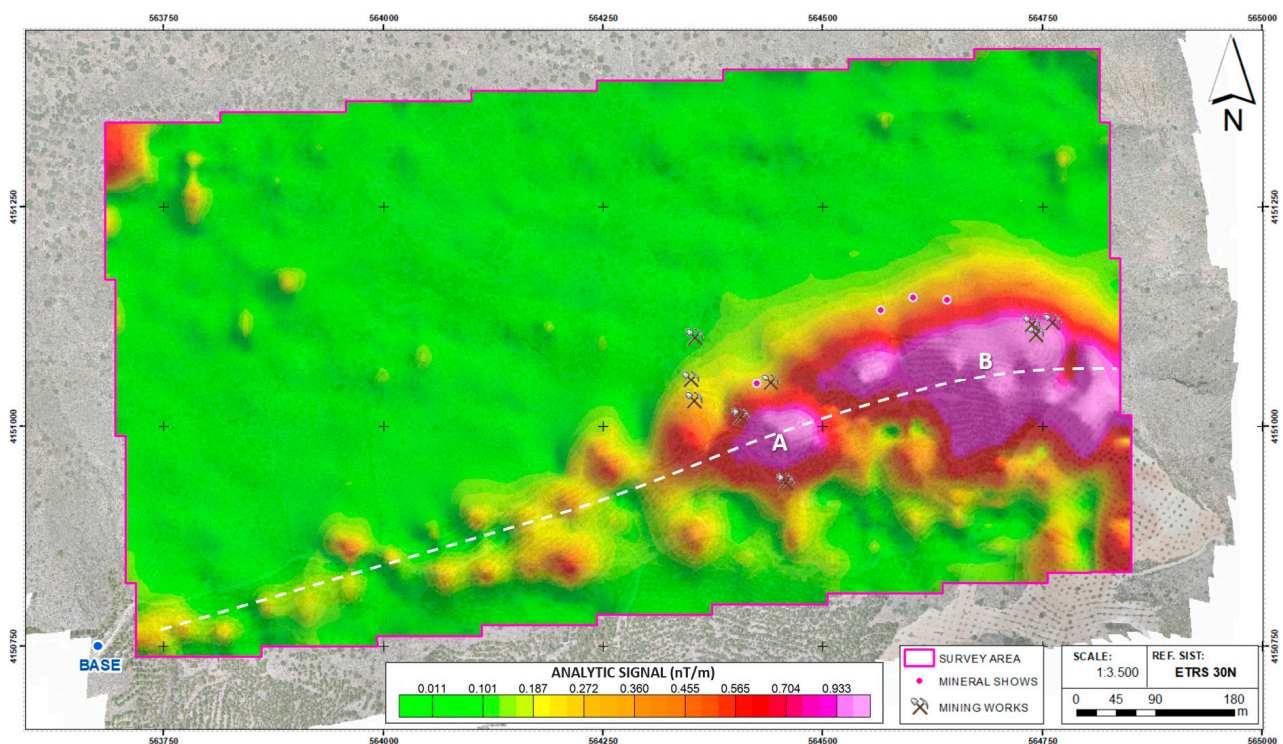


**Figure 7.** Analytical signal map over the aerial RGB image of the area of Don Jacobo with the position of the main mining works and outcropping mineral shows. Note the alignment of the analytical signal anomalies with approximate N80E orientation (white dashed line) and with the two AS maxima (A and B), as well as the position of the mining works and the outcropping mineral shows close to the main anomalies.

It is important to point out that all the mining works and outcropping mineral shows are located surrounding the northern part of the analytical signal anomalies, with all of them situated in the northern block of the normal fault.

### 4.3. D Inversion Model

The creation of a uniform grid with a high density of information obtained by drone allows to the creation of 3D models displaying magnetic susceptibility by applying the technique of Magnetic Vector Inversion (MVI) [30]. The model generated using the VOXI Earth Modeling software by OASIS Montaj is made up of a data mesh of $117 \times 69 \times 82$, generating a total of 661,986 cells of $10 \times 10$ m size. This model facilitated the spatial definition of the precise magnetic bodies of interest. These methods also allow for the characterization of these bodies, through computing magnetization vectors for each block that contain information about directionality as well as intensity.
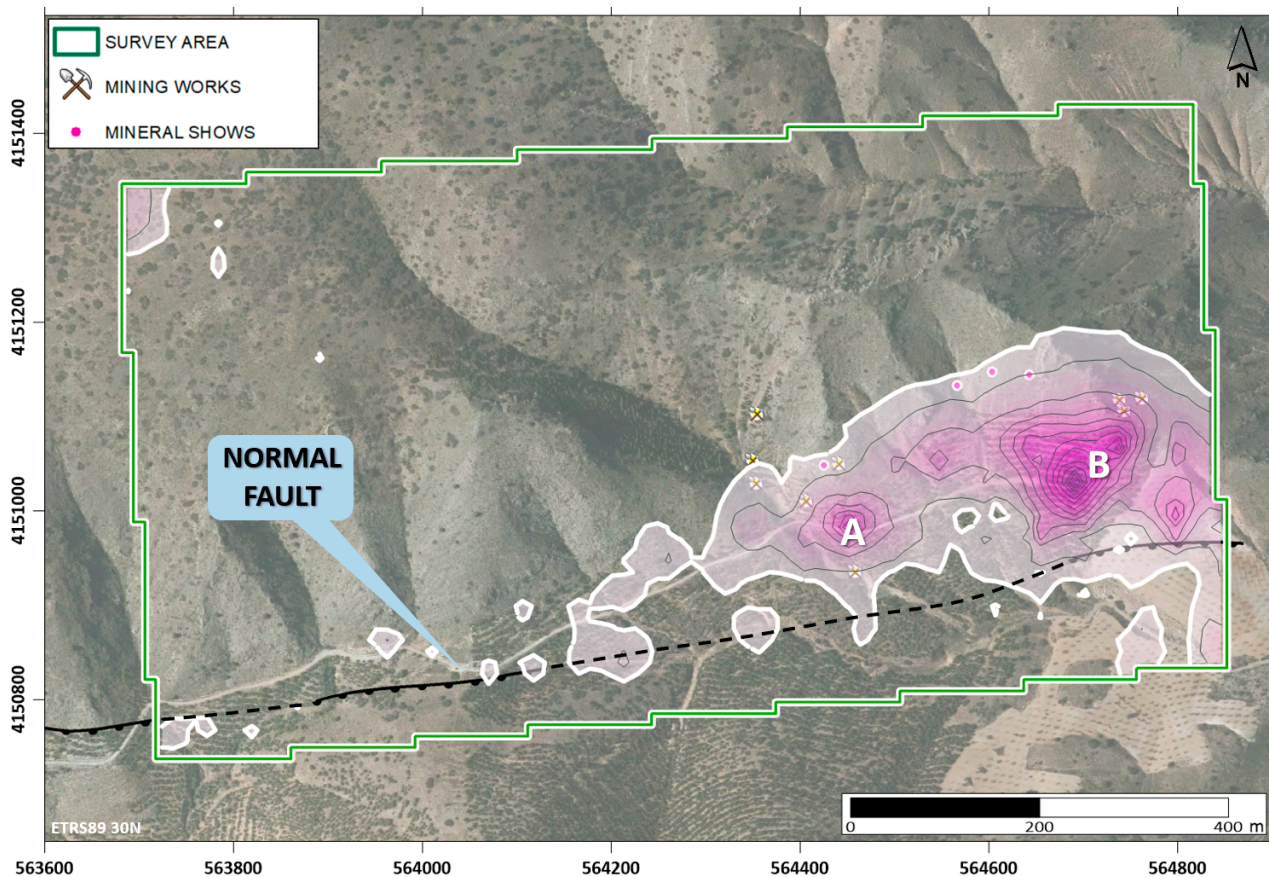


**Figure 8.** Analytical Signal anomalies over the aerial RGB image and normal fault trace from the 1:5000 geological cartography (Figure 1C) of the area of Don Jacobo. Note the alignment of analytical signal anomalies parallel to the normal fault placed at the south of the survey area.

The results from this modeling (Figure 9) reveals the presence of two bodies with high magnetic susceptibility (A and B), presenting susceptibility values over $12 \times 10^{-4}$, with peak values of $15 \times 10^{-3}$. Both bodies are modelled to prevent an oval morphology, with the maximal magnetization located at 45 m and 60 m in depth below surface (Figure 9A,B). This depth is an estimation and other methods such as drilling would be required to validate the proposed depth.

In the case of magnetization vectors, a preferential W-E orientation has been observed, different from the direction of the Earth's natural magnetic field. This model confirms the presence of a residual magnetization in the materials encountered here, coinciding with those observations obtained from TMFRP, and therefore, could be related to the presence of mineralized bodies.

Both bodies are located towards the south of the mining works and outcropping mineral shows and just at the north of the normal fault that crosses the southern border of the survey area (Figure 10), making it possible to interpret that the fault may have played

an important role in the formation of the mineralization, probably as a channel for the circulation of hydrothermal mineralizing fluids.
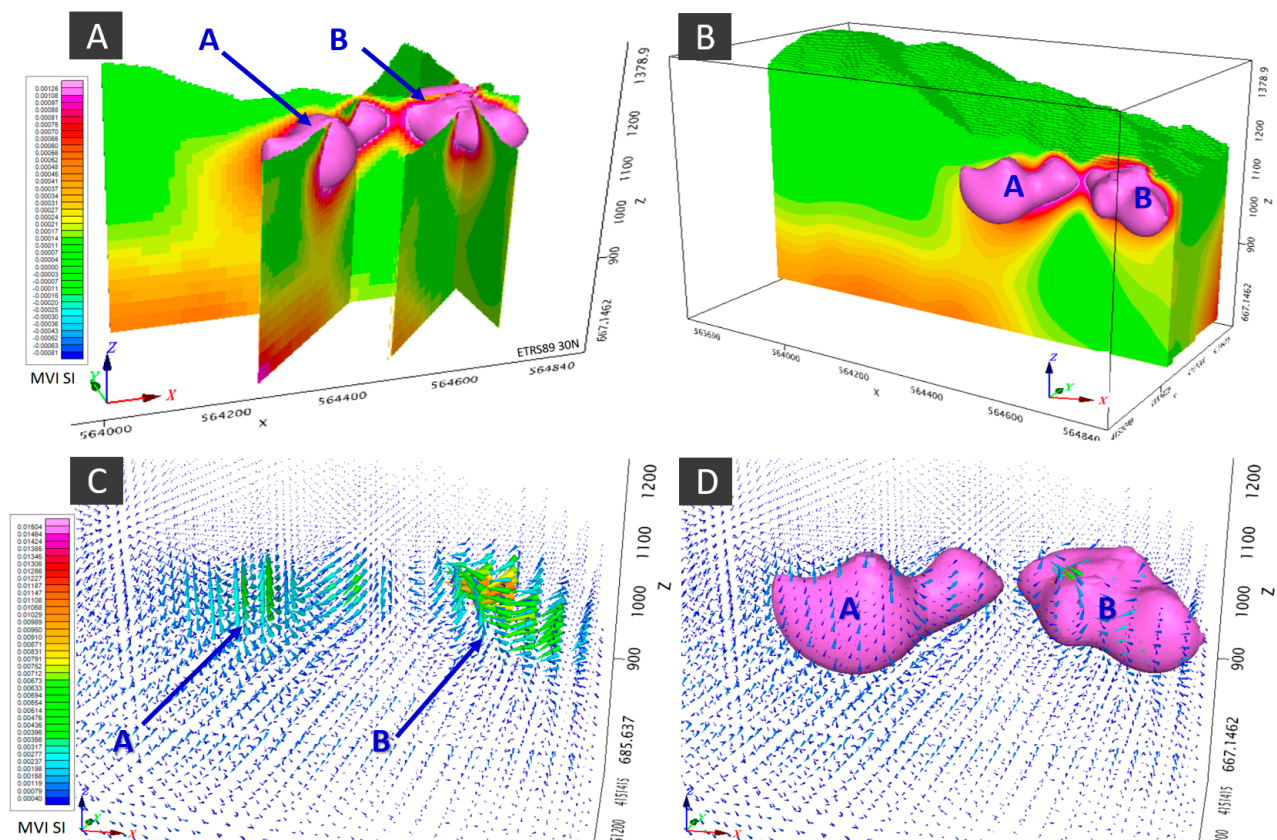


**Figure 9.** 3D model of the magnetic susceptibility in the area of Don Jacobo. (**A**,**B**) Different views and sections of the two magnetic bodies defined by the model. (**C**,**D**) Visualization of magnetization vectors obtained from each of the studies and their relationship with magnetic susceptibility.
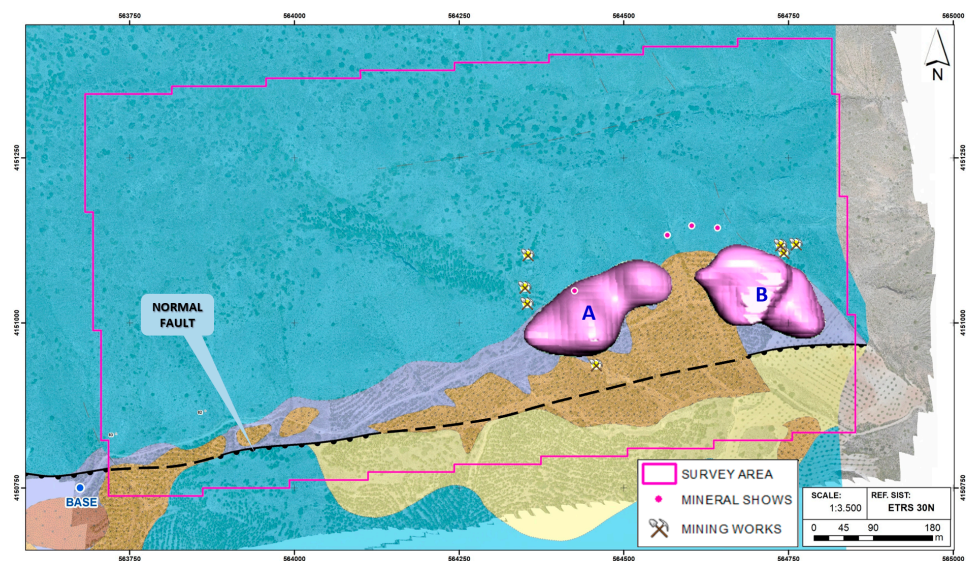


**Figure 10.** 3D model of the magnetic susceptibility of the Don Jacobo area, displaying the position of the two bodies of high magnetic susceptibility A and B ($12 \times 10^{-4}$ susceptibility threshold value); over the 1:5000 geological cartography and aerial RGB image of the area of Don Jacobo; normal fault placed at the south of the survey area and mining works and outcropping mineral shows.

## 5. Conclusions

We present results of the drone magnetometry survey for mineral exploration over the Don Jacobo mining area. We demonstrate the utility and advantages of using drone magnetometry in the study of mineral deposits, allowing for the acquisition of high-quality data in unfavorable conditions where traditional approaches are limited.

The present study was able to detect the presence of two magnetic dipoles with residuals magnetization in the nearby surroundings of old mining activities.

The use of 3D inversion was able to define the morphology and limits of the two potential mineral bodies, and further confirm their relation to the surrounding geological features, such as the normal fault to the south of the region of interest.

Our results strongly support that these dipoles are related to the potential presence of ferromagnetic mineral elements compatible with the Copper-Cobalt-Nickel paragenesis of the Don Jacobo area. The alignment of the analytical signal anomalies parallel and close to a normal fault indicate that this fault played an important role in the formation of the mineralization, probably as a channel for the circulation of hydrothermal mineralizing fluids.

We conclude that the drone magnetics survey method could be an important tool to study mineralized areas, such as the Don Jacobo mine, where precise modeling allows the precise definition of magnetic anomalies and the design and development of future investigation activities.

## References

1.  Giordan, D.; Adams, M.S.; Aicardi, I.; Alicandro, M.; Allasia, P.; Baldo, M.; De Berardinis, P.; Dominici, D.; Godone, D.; Hobbs, P.; et al. The use of unmanned aerial vehicles (UAVs) for engineering geology applications. *Bull. Eng. Geol. Environ.* **2020**, *79*, 3437–3481. [CrossRef]
2.  Aleshin, I.M.; Ivanov, S.D.; Koryagin, V.N.; Matveev, M.A.; Morozov, Y.A.; Perederin, F.V.; Kholodkov, K.I. Review on the Use of Light Unmanned Aerial Vehicles in Geological and Geophysical Research. *Seism. Instrum.* **2020**, *56*, 509–515. [CrossRef]
3.  Parvar, K.; Braun, A.; Layton-Matthews, D.; Burns, M. UAV magnetometry for chromite exploration in the Samail ophiolite sequence, Oman. *J. Unmanned Veh. Syst.* **2018**, *6*, 57–69. [CrossRef]
4.  Shahmoradi, J.; Talebi, E.; Roghanchi, P.; Hassanalian, M. A comprehensive review of applications of drone technology in the mining industry. *Drones* **2020**, *4*, 34. [CrossRef]
5.  Malehmir, A.; Dynesius, L.; Paulusson, K.; Paulusson, A.; Johansson, H.; Bastani, M.; Wedmark, P.; Marsden, P. The potential of rotary-wing UAV-based magnetic surveys for mineral exploration: A case study from central Sweden. *Lead. Edge* **2017**, *36*, 552–557. [CrossRef]
6.  Park, S.; Choi, Y. Applications of unmanned aerial vehicles in mining from exploration to reclamation: A review. *Minerals* **2020**, *10*, 663. [CrossRef]
7.  Kim, B.; Lee, S.; Park, G.; Cho, S.-J. Development of an unmanned airship for magnetic exploration. *Explor. Geophys.* **2020**, *52*, 1–6. [CrossRef]

8. Le Maire, P.; Bertrand, L.; Munschy, M.; Diraison, M.; Géraud, Y. Aerial magnetic mapping with an unmanned aerial vehicle and a fluxgate magnetometer: A new method for rapid mapping and upscaling from the field to regional scale. *Geophys. Prospect.* **2020**, *68*, 2307–2319. [CrossRef]

9. Schmidt, V.; Becken, M.; Schmalzl, J. A UAV-borne magnetic survey for archaeological prospection of a Celtic burial site. *First Break* **2020**, *38*, 61–66. [CrossRef]

10. Alex, N.; Timothy, S.d.S. A UAV-based magnetic survey method to detect and identify orphaned oil and gas wells. *Lead. Edge* **2019**, *38*, 447–452.

11. Hammack, R.W.; Veloski, G.A.; Lowe, R.; Zorn, A.; Wylie, L.; Schlagenhauf, M. *Using Drone-Mounted Geophysical Sensors to Map Legacy Oil and Gas Infrastructure*; National Energy Technology Laboratory (NETL): Pittsburgh, PA, USA; Medium: Morgantown, WV, USA, 2020.

12. De Smet, T.S.; Nikulin, A.; Romanzo, N.; Graber, N.; Dietrich, C.; Puliaiev, A. Successful application of drone-based aeromagnetic surveys to locate legacy oil and gas wells in Cattaraugus county, New York. *Appl. Geophys.* **2021**, *186*, 104250. [CrossRef]

13. Everett, M. *Near-Surface Applied Geophysics*; Cambridge University Press: Cambridge, UK, 2013.

14. Parvar, K. Development and Evaluation of Unmanned Aerial Vehicle (UAV) Magnetometry Systems. Master's Thesis, Department of Geological Sciences and Geological Engineering, Queen's University, Kingston, ON, Canada, 2016; pp. 1–141.

15. Parshin, A.; Morozov, V.; Blinov, A.; Kosterev, A.; Budyak, A. Low-altitude geophysical magnetic prospecting based on multirotor UAV as a promising replacement for traditional ground survey. *Geo-Spat. Inf. Sci.* **2018**, *21*, 1–8. [CrossRef]

16. Jackisch, R.; Madriz, Y.; Zimmermann, R.; Pirttijärvi, M.; Saartenoja, A.; Heincke, B.H.; Salmirinne, H.; Kujasalo, J.-P.; Andreani, L.; Gloaguen, R. Drone-borne hyperspectral and magnetic data integration: Otanmäki Fe-Ti-V deposit in Finland. *Remote Sens.* **2019**, *11*, 2084. [CrossRef]

17. Empresa Nacional Adaro de investigaciones Mineras (ADARO). *Programa de Investigación Sistemática de Recursos*; Zona Sureste, Sierra de Las Estancias; ADARO: Madrid, Spain, 1987.

18. IGME MAGNA; Instituto Geológico y Minero de España (IGME). *Hoja de Chirivel (973)*; Mapa Geológico de España (E. 1:50.000); Servicio de Publicaciones del Ministerio de Industria y Energía: Madrid, Spain, 1972; 46p.

19. IGME MAGNA; Instituto Geológico y Minero de España (IGME). *Hoja de Cantoria (995)*; Mapa Geológico de España (E. 1:50.000); Servicio de Publicaciones del Ministerio de Industria y Energía: Madrid, Spain, 1972; 51p.

20. EXCO MINING, SL. *Informe Geológico y Minero del Permiso de Investigación Burán*; Sierra de Oria, Informe Interno no Publicado; EXCO MINING SL: Madrid, Spain, 2019.

21. EXCO MINING, SL. *Análisis Geoquímico y Petrográfico de Muestras Superficiales Tomadas en el Permiso de Investigación Burán*; Informe Interno no Publicado; EXCO MINING SL: Madrid, Spain, 2020.

22. Hernandez-Lopez, D.; Felipe-Garcia, B.; Gonzalez-Aguilera, D.; Arias-Perez, B. An automatic approach to UAV flight planning and control for photogrammetric applications. *Photogramm. Eng. Remote Sens.* **2013**, *79*, 87–98. [CrossRef]

23. Cunningham, M.; Samson, C.; Wood, A.; Cook, I. Aeromagnetic Surveying with a Rotary-Wing Unmanned Aircraft System: A Case Study from a Zinc Deposit in Nash Creek, New Brunswick, Canada. *Pure Appl. Geophys.* **2018**, *175*, 3145–3158. [CrossRef]

24. Walter, C.A.; Braun, A.; Fotopoulos, G. Impact of three-dimensional attitude variations of an unmanned aerial vehicle magnetometry system on magnetic data quality. *Geophys. Prospect.* **2019**, *67*, 465–479. [CrossRef]

25. Jirigalatu, J.; Krishna, V.; Silva, E.; Døssing, A. Experiments on magnetic interference for a portable airbone magnetometry system using a hybrid unmanned aerial vehicle (UAV). *Geosci. Instrum. Methods Data Syst.* **2020**, *10*, 25–34. [CrossRef]

26. Telford, W.M.; Geldart, L.R.; Sheriff, R.E. *Applied Geophysics*, 2nd ed.; Cambridge University Press: Cambridge, UK, 1990; 770p.

27. Briggs, I.C. Machine contouring using minimum curvature. *Geophysics* **1974**, *39*, 39–48. [CrossRef]

28. Lee, M.; Morris, W. Quality assurance of aeromagnetic data using lineament analysis. *Explor. Geophys.* **2013**, *44*, 104. [CrossRef]

29. Nabighian, M.N.; Grauch, V.J.S.; Hansen, R.O.; LaFehr, T.R.; Li, Y.; Peirce, J.W.; Phillips, J.D.; Ruder, M.E. The historical development of the magnetic method in exploration. *Geophysics* **2005**, *70*, 33–61. [CrossRef]

30. MacLeod, I.N.; Ellis, R.G. Magnetic Vector Inversion, a Simple Approach to the Challenge of Varying Direction of Rock Magnetization. Australian Society of Exploration Geophysicists, Extended Abstracts. 2013, pp. 1–4, Melbourne. Available online: https://www.semanticscholar.org/paper/Magnetic-Vector-Inversion-%2C-a-simple-approach-to-of-Macleod-Ellis/9cd186fe7e6843baeb43c706d80fc64ffed3109a (accessed on 1 December 2021).